frontiers | Frontiers in Marine Science

TYPE Original Research
PUBLISHED 07 March 2025
DOI 10.3389/fmars.2025.1513219

Check for updates

OPEN ACCESS

EDITED BY
Xia Wang,
Chengdu University of Technology, China

REVIEWED BY
Yiwei Xu,
Chinese Academy of Sciences (CAS), China
Fayao Chen,
SINOPEC, China

*CORRESPONDENCE
Xuefei Yi
yxf@yangtzeu.edu.cn

RECEIVED 18 October 2024
ACCEPTED 24 February 2025
PUBLISHED 07 March 2025

CITATION
Huang Z, Yi X, Huang Y, Tian L, Wu K and Li M (2025) Response of carbonate factories to late Paleozoic climate change: a case study from the Yanduhe section, Hubei Province, South China.
Front. Mar. Sci. 12:1513219.
doi: 10.3389/fmars.2025.1513219

COPYRIGHT
© 2025 Huang, Yi, Huang, Tian, Wu and Li. This is an open-access article distributed under the terms of the Creative Commons Attribution License (CC BY). The use, distribution or reproduction in other forums is permitted, provided the original author(s) and the copyright owner(s) are credited and that the original publication in this journal is cited, in accordance with accepted academic practice. No use, distribution or reproduction is permitted which does not comply with these terms.

Response of carbonate factories to late Paleozoic climate change: a case study from the Yanduhe section, Hubei Province, South China

Zihang Huang[1], Xuefei Yi[1]*, Yunfei Huang[1], Li Tian[2], Kui Wu[3] and Mengfan Li[1]

[1]School of Geosciences, Yangtze University, Wuhan, China, [2]State Key Laboratory of Biogeology and Environmental Geology, China University of Geosciences, Wuhan, China, [3]Hubei Key Laboratory of Resource and Eco-Environment Geology, Hubei Institute of Geosciences, Hubei Geological Bureau, Wuhan, China

The carbonate factory concept was proposed to understand the spatial dynamics and processes involved in carbonate production, which was heavily influenced by climate change. The Permian period witnessed several significant climate change events that had a considerable impact on the carbonate factory. However, research on how the carbonate factory responded to these climate change events during the Permian is still limited. In this study, a detailed analysis of carbonate microfacies was conducted in the Yanduhe section, western Hubei Province, South China, to investigate the relationship between the carbonate factory and climate change. Ten sedimentary microfacies were detected, and classified into three microfacies associations, which correspond to different environments of inner ramp, middle ramp, and outer ramp. Meanwhile, eight transgression-regression sequences were identified, revealing a sea-level change trend consistent with observations from other regions in South China. Furthermore, six types of carbonate factories were recognized and five changes in carbonate factories were observed. Among those five changes, two occurred during the Late Kungurian and Late Wuchiapingian respectively, and may be attributed to climate changes, while one at the end-Guadalupian likely resulted from both the end-Guadalupian mass extinction and climate change. The other two changes in carbonate factories were caused by sea-level fluctuations. In addition, climate change affects sea surface temperature and sea levels, thereby regulating the biological communities involved in carbonate production and driving a shift in the types of carbonate factories.

KEYWORDS

Permian, carbonate factory, carbonate microfacies, sedimentary environment, climate change

1 Introduction

Carbonate rocks are one of the most abundant sedimentary deposits in Earth's history and their formation processes and environments have received considerable attention for decades (Laugie et al., 2019; Reijmer, 2021; Wang J. Y. et al., 2023). Since the beginning of the 21st century, the concept of carbonate factories has been widely used to summarize the environments and processes involved in the production of these rocks (e.g., Schlager, 2003; Pomar and Hallock, 2008; Eynattern and Dunkl, 2012; Michel et al., 2019; Reijmer, 2021; Li et al., 2024). Moreover, various types of carbonate factories have been categorized, such as T-factory, C-factory, M-factory, P-factory, and Ooid-factory (Schlager, 2003; Pomar and Hallock, 2008; Pomar and Haq, 2016; Li F. et al., 2019; Reijmer, 2021). Several key factors have been proposed to influence the development of different carbonate factories, such as climate, light availability, temperature, nutrient conditions, salinity, carbonate saturation, ocean currents, and sea-level changes (Reijmer, 2021; Wang et al., 2024). Among these factors, climate change has played a significant role in carbonate production throughout the Earth's history (e.g., Krencker et al., 2014; Li F. et al., 2019, Li et al., 2023; Lehrmann et al., 2022; Morabito et al., 2024). In the Atlas Rift Basin of Morocco, a decrease in sea surface temperature during the Middle to Late Tournaisian led to the demise of the ooid carbonate factory (Krencker et al., 2014). During the Permian-Triassic age, metazoan-dominated carbonate factories transitioned to benthic automicrite factories, ooid factories and microbial-induced factories in association with global warming (Li F. et al., 2019; Li M. T. et al., 2019, Li et al., 2023; Lehrmann et al., 2022). The cooling following the Middle Eocene Climate Optimum Event in the Apulia carbonate platform of the Gargano region of southern Italy resulted in a shift from a benthic foraminifers-dominated carbonate factory to a corals-dominated one (Morabito et al., 2024).

The Permian (the last epoch of the Late Paleozoic) is one of the most crucial periods in geological history, marked by a series of biological and environmental events (Shen et al., 2019, Shen et al., 2024; Song et al., 2023; Wang W. Q. et al., 2023). These include the eruption of the Emeishan Large Igneous Province (Shellnutt et al., 2020; Wei C. et al., 2024), oceanic anoxic events (He et al., 2022; Song et al., 2023), the transition between icehouse and greenhouse climates (Marchetti et al., 2022; Hou et al., 2023), mass extinction events (Qiu et al., 2014; Shen and Zhang, 2017), and sea-level changes (Lestari et al., 2024; Qiu et al., 2024), all of which significantly impacted carbonate production. Previous studies have demonstrated that carbonate platforms in South China underwent a substantial reduction during the Middle Permian (Meng et al., 2022; Lei et al., 2024), which was associated with the replacement of deep-water carbonate rocks by siliceous rocks (e.g., Qiu et al., 2014, Qiu et al., 2024; Shen et al., 2020). In addition, the eruption of the Emeishan Large Igneous Province caused the upper Yangtze platform exposed, leading to a stratigraphic gap (Meng et al., 2018, Meng et al., 2022; Liu et al., 2023). These phenomena suggest significant changes in carbonate factories during the Middle Permian, likely linked to the Late Paleozoic climate changes or sea-level fluctuations. However, studies on how carbonate factories responded to climate changes during the Permian are still rare. In this study, the continuous development of Early-Late Permian carbonate sediments from the Yanduhe section provides a good window to evaluate the evolution of carbonate factories. This study aims to identify carbonate microfacies, analyze environmental changes, classify carbonate factory types, and discuss the driving factors influencing the evolution of carbonate factories in the Yanduhe section, Hubei Province.

2 Geological setting

During the Early to Late Permian period, the South China Block was located in the eastern part of the Paleo-Tethys Ocean, flanked by old-lands to the east and west (Wang and Jin, 2000; Wei et al., 2016). Various paleogeographic units have been recognized, including the Yangtze Platform, the Cathaysia Platform, the North Yangtze Basin, the Nanpanjiang Basin, the Qianzhong Intrashelf Basin, the Jiangnan Basin, the Kangtian Old Land and the Cathaysia Old Land (Figure 1A). Among them, the North Yangtze Basin represents a typical deep-water basin environment, encompassing areas in western and northern Hubei Province, northern Jiangxi Province, northern Anhui Province and northern Jiangsu Province (Wang and Jin, 2000; Wei et al., 2016).

The Yanduhe section (GPS: 31°13′06″ N, 110°18′09″ E) is located in Yanduhe Town, Badong County, Enshi Tujia and Miao Autonomous Prefecture, Hubei Province (Figure 1B). The continuous stratigraphic successions of the Permian and Lower Triassic can be divided into the Liangshan, Qixia, Maokou, Wujiaping, and Dalong formations in ascending order (Figure 1C), with a total thickness of about 500 meters. The Liangshan Formation consisting of coal-bearing clastic rock, is unconformable contacted with the underlying strata. The Qixia Formation is characterized by dark-gray to black-gray, thin- to medium-bedded argillaceous limestone that are rich in non-fusulinid foraminifers and brachiopods, with a thickness of about 90.8 meters (Figure 2A). The Maokou Formation is consist of black-gray thick-bedded cherty bioclastic limestone containing abundant non-fusulinid foraminifers and calcareous algae fossils, 295 meters in totally (Figure 2C). The Wujiaping Formation comprises gray thick-bedded, chert-bearing bioclastic limestone, with a thickness of about 101 meters (Figures 2D, E). The Dalong Formation includes black-gray thin-bedded argillaceous limestone, siliceous-carbonaceous shale, and carbonaceous mudstone (Figure 2F). It is overlain by the thin-bedded limestone of the Lower Triassic Daye Formation.

According to the conodont biostratigraphic framework of the Yanduhe section (Figure 1; Wu, 2020), the first appearance of the conodont *Jinogondolella nankingensis* occurs 29 meters above the base of the Maokou Formation, marking the base of the Roadian stage and the base of the Guadalupian series (Figure 3). The first occurrence of *Jinogondolella aserrata* occurs 70.8 meters above the Maokou Formation base, indicating the beginning of the Wordian stage (Figure 3). The first occurrence of *Jinogondolella postserrata*

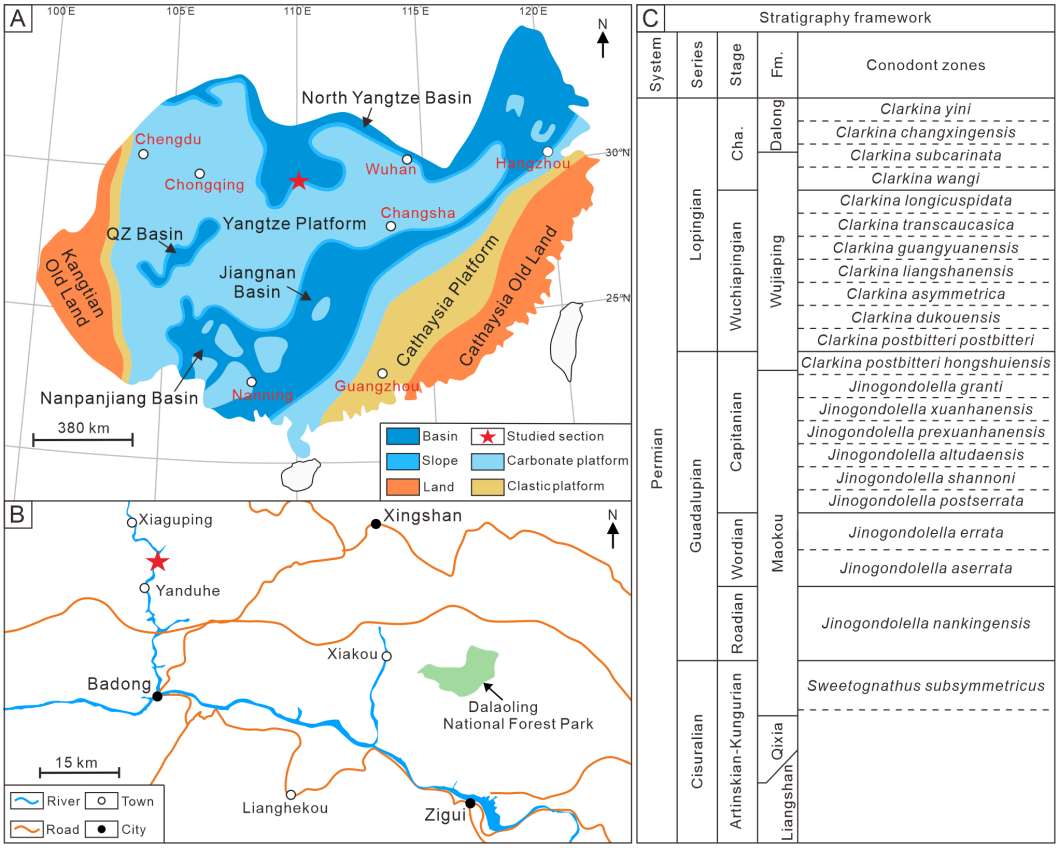

FIGURE 1
Middle Permian (Capitanian) paleogeography of South China and Permian stratigraphy framework of the Yanduhe section. **(A)** Middle Permian (Capitanian) paleogeography of South China (modified after Wang et al., 2020 and Wei et al., 2016); **(B)** Location map of the Yanduhe section; **(C)** Permian stratigraphy of the Yanduhe section. QZ Basin, Qianzhong Intrashelf Basin; Fm., Formation; Cha., Changhsingian.

occurs 104.2 meters, marking the onset of the Capitanian stage (Figure 3). The first appearance of the conodont *Clarkina postbitteri postbitteri* occurs 13 meters above the Wujiaping Formation base, indicating the base of the Wuchiapingian stage and the base of the Lopingian series (Figure 3). And the first occurrence of *Clarkina wangi* occurs 77.6 meters above Wujiaping Formation base, marking the Changhsingian stage beginning (Figure 3).

3 Materials and methods

A total of 252 rock samples were collected at intervals ranging from 0.5 to 3 meters in the Qixia, Maokou, and Wujiaping formations. These samples were processed in the laboratory to make thin sections of rock. A Zeiss AxioScope A1 polarizing microscope was employed for a detailed examination of grain types, grain abundances, support types, and cement characteristics. Following the carbonate rock classification scheme established by Dunham (1962) and Embry and Klovan (1971), the carbonate rocks from the Yanduhe section were categorized into six types: mudstone, wackestone, packstone, grainstone, floatstone and rudstone. The carbonate microfacies and sedimentary environments along this section were further classified and analyzed based on differences in grain composition, matrix type, fossil types, and other characteristics. In addition, a quantitative analysis of bioclast content was conducted for each rock section using point counting methods (Flügel, 2004). For limestone with varying particle sizes and poor sorting, it is recommended to count more than 1000 points (Flügel, 2004). In this study, a total of 1024 points were counted within an area of 5.5 mm×3.5 mm, and the relative abundances of different bioclasts were counted for all thin sections (Supplementary Table 1).

4 Results

4.1 Carbonate microfacies

A total of ten microfacies were identified and grouped into three associations that correspond to inner ramp, middle ramp, and outer ramp environments (Figures 3, 4). Consequently, the study area may represent a carbonate ramp depositional model (Figure 5).

4.1.1 Inner ramp microfacies association

4.1.1.1 MF1: Bioclasts grainstone

This microfacies occurs in the middle to upper part of the Maokou Formation and the middle part of the Wujiaping

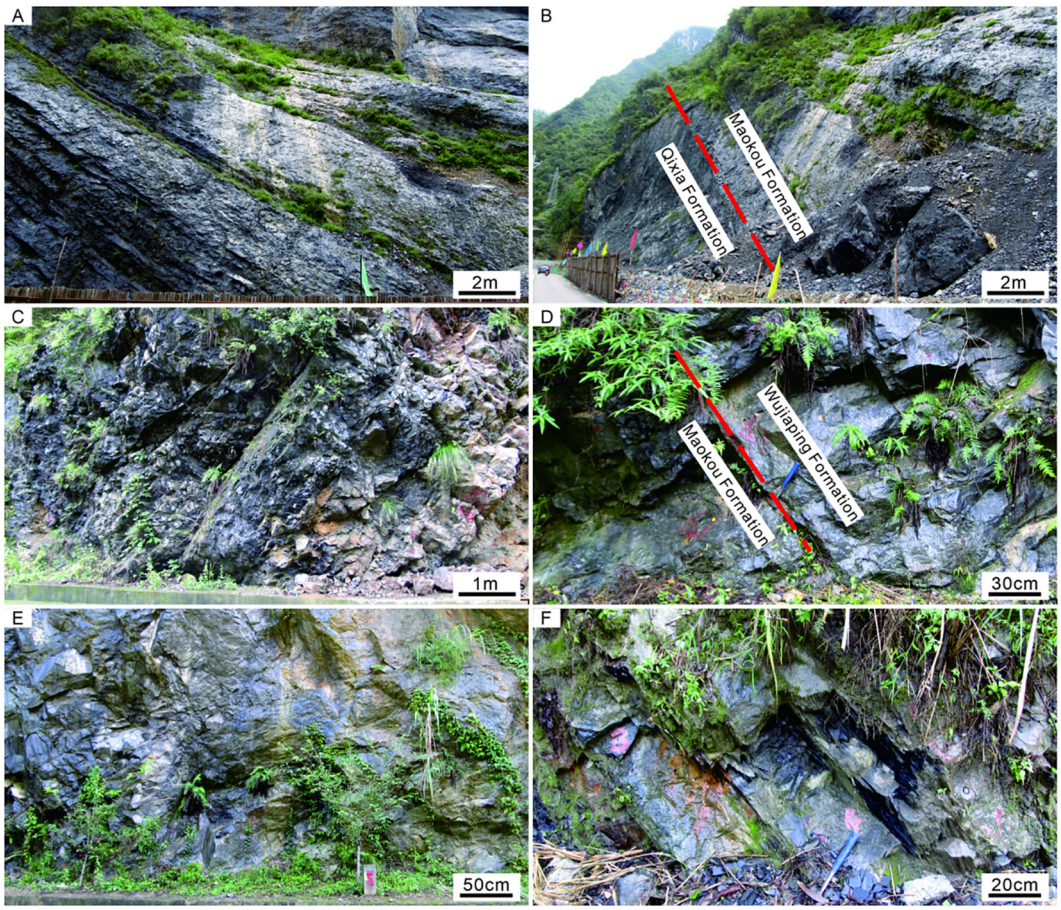

FIGURE 2
Field photos of the Yanduhe section. **(A)** Thin to Medium-bedded argillaceous limestone of the Qixia Formation; **(B)** Boundary between the Qixia Formation and the Maokou Formation; **(C)** Thick-bedded cherty bioclastic limestone of the Maokou Formation; **(D)** Boundary between the Maokou Formation and the Wujiaping Formation; **(E)** Gray thick-bedded, chert-bearing bioclastic limestone of the Wujiaping Formation; **(F)** Argillaceous limestone, siliceous-carbonaceous shale, and carbonaceous mudstone of the Dalong Formation.

Formation (Figure 3). Grains make up 35%~40% of the thin sections (Figures 4A, B). The dominant grains are bioclasts, displaying a relatively high diversity of fossils, including tubiphytes, non-fusulinid foraminifers, crinoids, fusulinids, algae, and gastropods, which collectively account for 30%~35% (Figure 4A). Some bioclasts exhibit micrite envelopes (Figure 4A). MF1 is grain-supported with sparite cement (Figures 4A, B), which indicates high energy above the fair weather wave base. This microfacies likely represents the inner ramp environment (Figure 5).

4.1.2 Middle ramp microfacies association

4.1.2.1 MF2: coral floatstone

This microfacies only appears in the middle of the Wujiaping Formation (Figure 3). MF2 is primarily composed of micrite, with grains accounting for only 15%~25% of the thin sections (Figures 4C, D). The grains consist mainly of corals and sponges, associated with rare gastropods, ostracods, and crinoids (Figures 4C, D). Both corals and sponges are typically larger than 2 mm, with some exceeding 6 mm in size (Figures 4C, D). The high content of the micrite matrix clearly suggests deposition below the fair weather wave base. The presence of gravel-sized bioclasts may be attributed to storm action.

4.1.2.2 MF3: crinoids packstone

This microfacies concentrates in the middle and upper part of the Wujiaping Formation (Figure 3). Grains account for 40%~50% of the composition, predominantly consisting of crinoids, with grain sizes typically ranging from 1 mm to 2 mm (Figure 4E). Minor components include bioclasts such as bivalves, non-fusulinid foraminifers, algae, and coral fragments. MF3 is grain-supported with a micritic matrix, and the contacts among grains show point and convex interactions (Figure 4E). The micritic matrix and the poor size sorting of the crinoid grains suggest weak hydrodynamic conditions below the fair weather wave base.

4.1.2.3 MF4: bivalves rudstone

This microfacies is only found at the base of the Maokou Formation (Figure 3). Grains account for 25%~35% of the composition, primarily consisting of bivalves larger than 2 mm (Figure 4F). A small amount of non-fusulinid foraminifers,

10.3389/fmars.2025.1513219

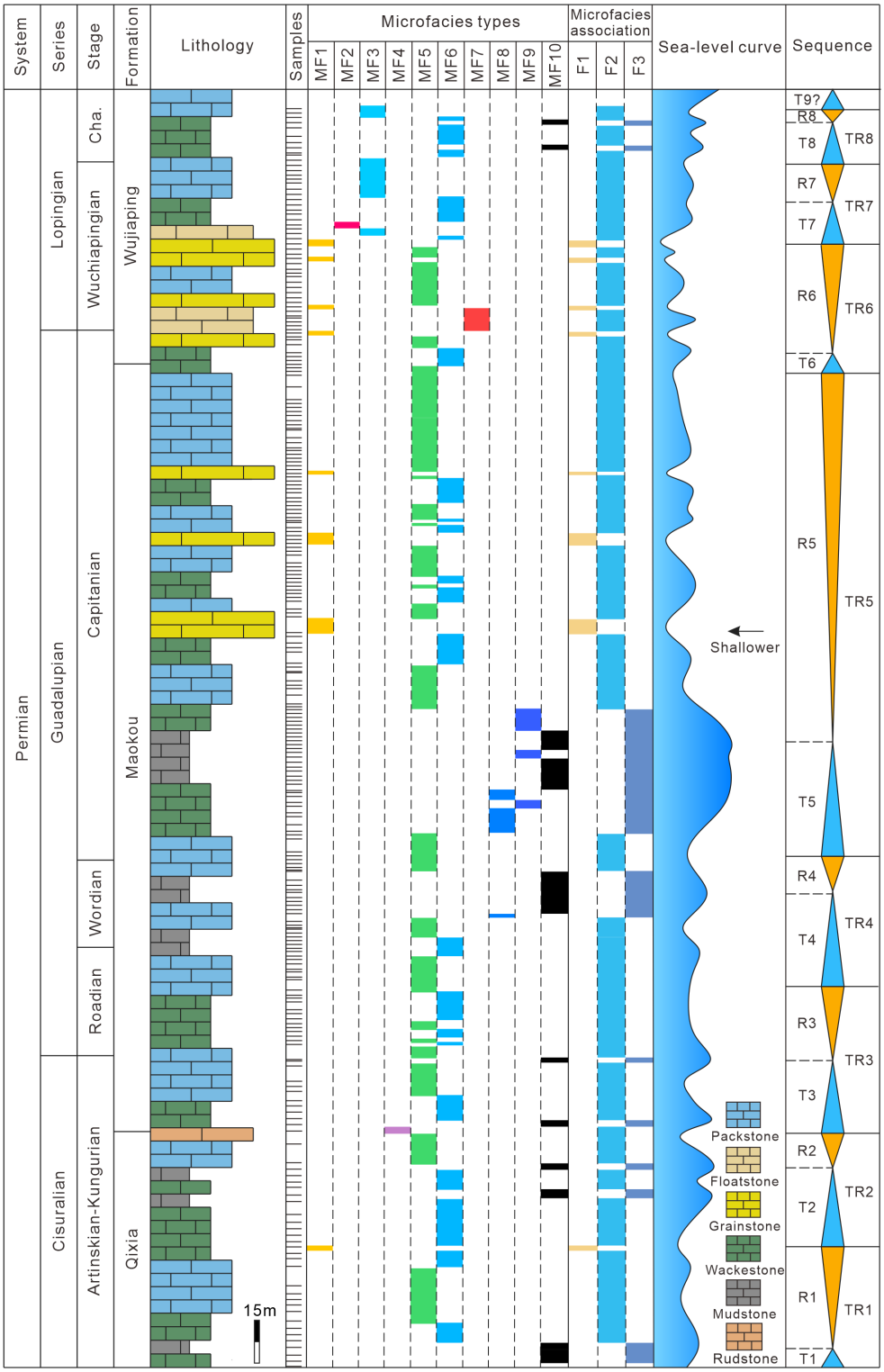

FIGURE 3
The sedimentary microfacies, microfacies association, and sea-level curve of the Yanduhe section. MF1, Bioclasts grainstone; MF2, Corals floatstone; MF3, Crinoids packstone; MF4, Bivalves rudstone; MF5, Bioclasts packstone; MF6, Bioclasts wackestone; MF7, Bioclasts floatstone; MF8, Calcispheres wackestone; MF9, Sponge spicules wackestone; MF10, Mudstone; F1, Inner ramp; F2, Middle ramp; F3, Outer ramp; TR, Transgressive-regressive sequence; Cha., Changhsingian.

10.3389/fmars.2025.1513219

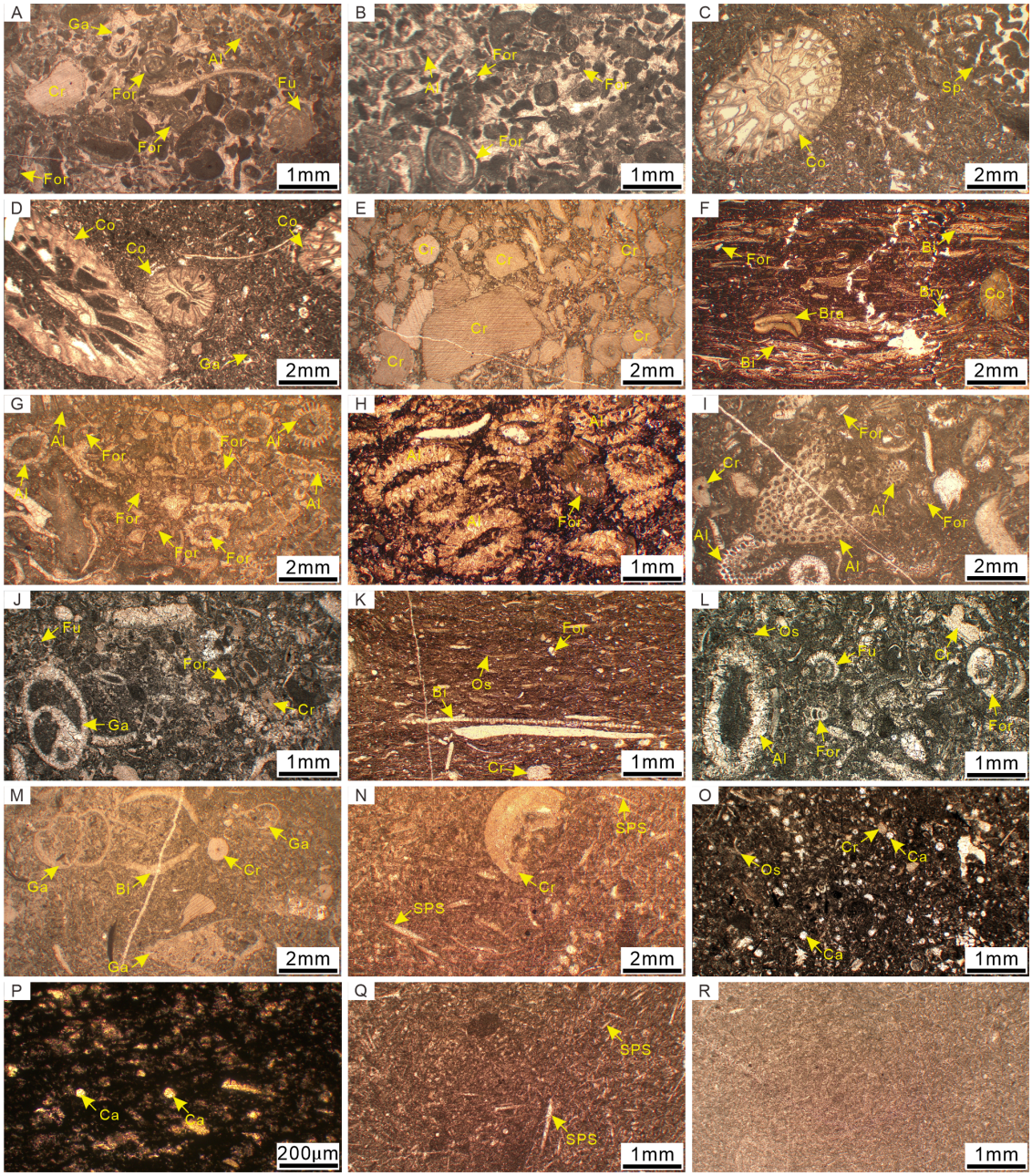

FIGURE 4
Microphotograph of different microfacies in the Yanduhe section. **(A-B)** Bioclasts grainstone; **(C-D)** Corals floatstone; **(E)** Crinoids packstone; **(F)** Bivalves rudstone; **(G-I)** Bioclasts packstone; **(J-L)** Bioclasts wackestone; **(M-N)** Bioclasts floatstone; **(O-P)** Calcispheres wackestone; **(Q)** Sponge spicules wackestone; **(R)** Mudstone microfacies; Ca, Calcisphere; SP, Sponge; Os, Ostracods; For, Foraminifer; Bi, Bivalve; Cr, Crinoid; Bra, Brachiopod; Ga, Gastropod; Bry, Bryozoan; AL, Algae; Fu, Fusulinid; Co, Coral; SPS, Sponge spicules.

brachiopods, bryozoans and corals are also observed (Figure 4F). MF4 is grain-supported with a micritic matrix (Figure 4F).

4.1.2.4 MF5: bioclasts packstone

This microfacies is distributed throughout the section. Grains make up 30%~35% of the thin sections (Figures 4G–I). The grains mainly consist of bioclasts, which include algae, non-fusulinid foraminifers, fusulinids, crinoids, ostracods, and sponges (Figures 4H–J). The grains are poorly sorted, with an average size of about 1 mm (Figures 4G–I). A small quantity of conglomerate bioclasts are observed. This microfacies is grain-supported with a micritic matrix (Figures 4G–I). The high micrite content indicates a low-energy sedimentary environment below the fair-weather wave base. The abundant fusulinids and algae indicate shallow water.

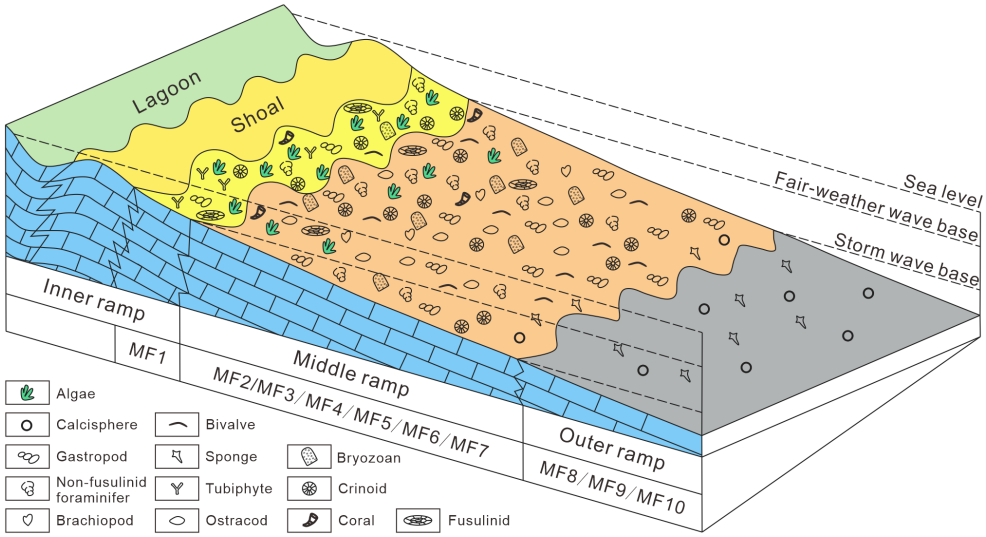

FIGURE 5
The sedimentary model of the Yanduhe section (modified after Burchette and Wright, 1992). The names of the microfacies (MF1~MF10) are the same as those in Figure 3.

4.1.2.5 MF6: bioclasts wackestone

This microfacies is also distributed throughout the section and is characterized by a dominance of micrite, with grains accounting for only 20%~30% (Figures 4J–L). Bioclasts are the primary grains, comprising non-fusulinid foraminifers, fusulinids, crinoids, algae, and ostracods (Figures 4J–L). The presence of bioturbation was noted, as the burrows were filled with bioclasts, indicating weak hydrodynamic conditions.

4.1.2.6 MF7: bioclasts floatstone

This microfacies only occurs at the base of the Wujiaping Formation (Figure 3). MF7 is dominated by micrite, with bioclasts accounting for only 15%~20% of the composition (Figures 4M, N). Bivalves and gastropods are the dominant bioclasts (Figure 4M), with rare occurrences of crinoids and sponges (Figure 4N). The grain sizes of bivalves and gastropods exceed 2 mm, accounting for 10%~15% (Figure 4M). The average size of the other bioclasts is between 0.5mm and 1 mm (Figure 4N). The high micrite content suggests a sedimentary environment located below the fair weather wave base, and the presence of gravel-sized bioclasts may also be related to storm action.

MF2 to MF7 are interpreted to represent environment of middle ramp (Figure 5).

4.1.3 Outer ramp microfacies association

4.1.3.1 MF8: calcispheres wackestone

This microfacies is distributed in the lower and middle part of the Maokou Formation (Figure 3). It is primarily composed of micrite, with grains constituting about 20%~25% (Figures 4O, P). The grain size is generally small, typically less than 200 μm (Figures 4O, P). Calcispheres are the dominant bioclasts, with rare contributions from crinoids, ostracods and non-fusulinid foraminifers, which together make up approximately 5% of the composition (Figure 4O). The high content of micrite, small fossils sizes, and scarcity of shallow water bioclasts imply weak hydrodynamics occurring below the storm wave base.

4.1.3.2 MF9: sponge spicules wackestone

This microfacies is present in the middle part of the Maokou Formation (Figure 3). Bioclasts account for 20%~25% of the thin section, with sponge spicules prevalent (Figure 4Q). The grain size is generally less than 0.5 mm. Some bioclasts have dissolved without recrystallisation. MF9 is mainly composed of micrite, indicating a low-energy sedimentary environment (Figure 4Q). The low abundance of shallow water bioclasts indicates a deep water sedimentary environment.

4.1.3.3 MF10: mudstone

This microfacies is distributed at the base of the Qixia Formation and the middle of the Maokou Formation (Figure 3). MF10 consists primarily of homogeneous micrite, with grains accounting for less than 5% of the composition (Figure 4R). The grains mainly comprise bioclasts, including sponge spicules, gastropods, and crinoids. A small amount of bioclasts have undergone dissolution and recrystallization. The presence of homogeneous micrite indicates a still water environment below the storm wave base.

MF8 to MF10 are interpreted to suggest an outer ramp environment (Figure 5).

4.2 Relative abundance of bioclasts

Bioclast types are diverse, including bivalves, gastropods, tubiphytes, crinoids, sponges, algae, non-fusulinid foraminifers,

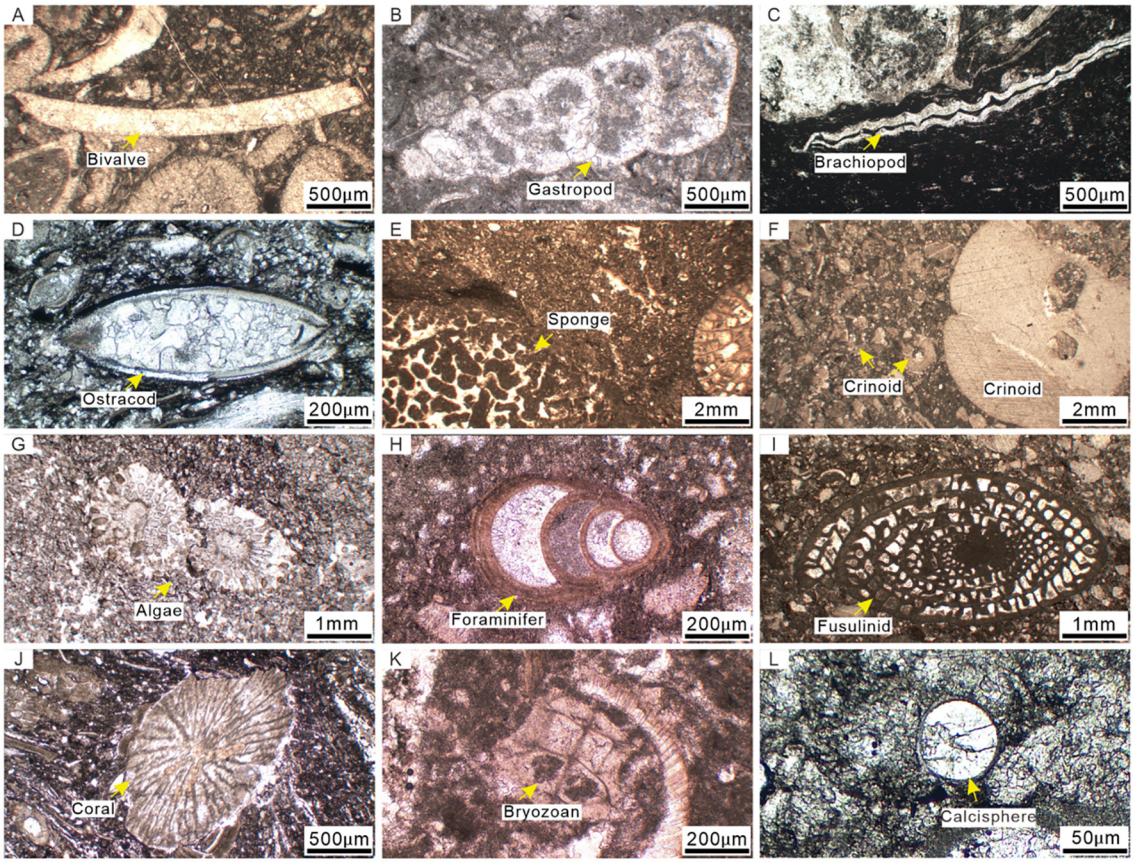

FIGURE 6
The different types of the bioclasts from the Yanduhe section. **(A)** Bivalves; **(B)** Gastropod; **(C)** Brachiopod; **(D)** Ostracod; **(E)** Sponge; **(F)** Crinoid; **(G)** Algae; **(H)** Foraminifer; **(I)** Fusulinid; **(J)** Coral; **(K)** Bryozoan; **(L)** Calcisphere.

fusulinids, corals, brachiopods, calcispheres, ostracods, and bryozoans (Figure 6). Throughout the Yanduhe section, there are significant changes in both the diversity and relative abundance of bioclasts from the bottom to the top. In the Kungurian stage, the relative abundance of bioclasts ranges from 15% to 25%, with abundant algae, ostracods, non-fusulinid foraminifers, bryozoans, and crinoids (Figure 7). In the Roadian to Lower Wordian stage, the bioclasts content increases to 15%~30%, although the overall diversity does not change significantly, with a small appearance of calcispheres (Figure 7). During the Upper Wordian to the Lower Capitanian stage, the relative abundance of bioclasts increases to 15%~30% again, but is dominated only by calcispheres and sponge spicules (Figure 7). In the Upper Capitanian stage, the bioclasts amount gradually increases to 20%~40%, featuring abundant tubiphytes, algae, and fusulinids. Algae account for about 10%~25% of the grains, while fusulinids make up approximately 5% to 15% (Figure 7). In the Wuchiapingian stage, the relative abundance of bioclasts ranges from 35% to 50% and is dominated by crinoids and non-fusulinid foraminifers, which together account for about 25% ~40% (Figure 7). In the Changhsingian stage, the bioclasts content also ranges from 35% to 50%, primarily consisting of conglomerate crinoids (Figure 7).

4.3 Carbonate factories

Six types of carbonate factories have been identified in the Yanduhe section (Figure 7):

4.3.1 Cool-water factory type A

This factory is distributed in the Qixia Formation and the lower part of the Maokou Formation (Artinskian-Kungurian age). It is dominated by ostracods, crinoids, non-fusulinid foraminifers, algae and bryozoans, which account for an average content of 24%, 19%, 16%, 15%, and 11% respectively, but lacks fusulinids and corals (Figure 7). The cool-water factory type A mainly consists of calcareous heterozoan, which are the primary carbonate producers of this factory.

4.3.2 Tropical factory type A

This one is located in the lower part of the Maokou Formation (Late Kungurian to Early Capitanian age), spanning the conodont zones from *Sweetognathus subsymmetricus* to *Jinogondolella shannoni*. This factory mainly consists of calcareous algae, crinoids, ostracods, and non-fusulinid foraminifers (Figure 7).

Algae and crinoids are the principal ones among them, accounting for 35% and 21% of the total content of bioclasts, respectively (Figure 7).

4.3.3 Cool-water factory type B

This factory is located in the middle part of the Maokou Formation (Early Capitanian age), spanning the conodont zones from *Jinogondolell shannoni* to *Jinogondolella altudaensis*. The Cool-water factory type B primarily consists of sponge and calcispheres (Figure 7). Among them, sponges make up 45%, and calcispheres account for 37% of the total content of bioclasts (Figure 7).

4.3.4 Tropical factory type B

This factory is distributed in the upper part of the Maokou Formation (Middle and Late Capitanian age), ranging from the conodont *Jinogondolella altudaensis* zone to the *Clarkina postbitteri hongshuiensis* zone. The tropical factory type B is characterized by abundant algae and fusulinids, in association with non-fusulinid foraminifers, crinoids, and ostracods (Figure 7). Of these organisms, algae and fusulinids comprise 44%, crinoids take up 20%, while non-fusulinid foraminifers make up 13% of the total content of bioclasts (Figure 7). It mainly consists of calcareous photozoan associations, with algae and fusulinids serving as the main carbonate producers.

4.3.5 Cool-water factory type C

This type of factory is located in the lower part of the Wujiaping Formation (Early to Late Wuchiapingian age), ranging from the conodont *Clarkina postbitteri postbitteri* zone to the *Clarkina longicuspidata* zone. The cool-water factory type C is dominated by crinoids and non-fusulinid foraminifers, with minor contributions from algae, bivalves, ostracods and brachipods (Figure 7). Within this organism association, crinods constitute 53% and non-fusulinid foraminifers occupy 13% of the total of the total content of bioclasts (Figure 7). Fusulinids disappeared in this factory.

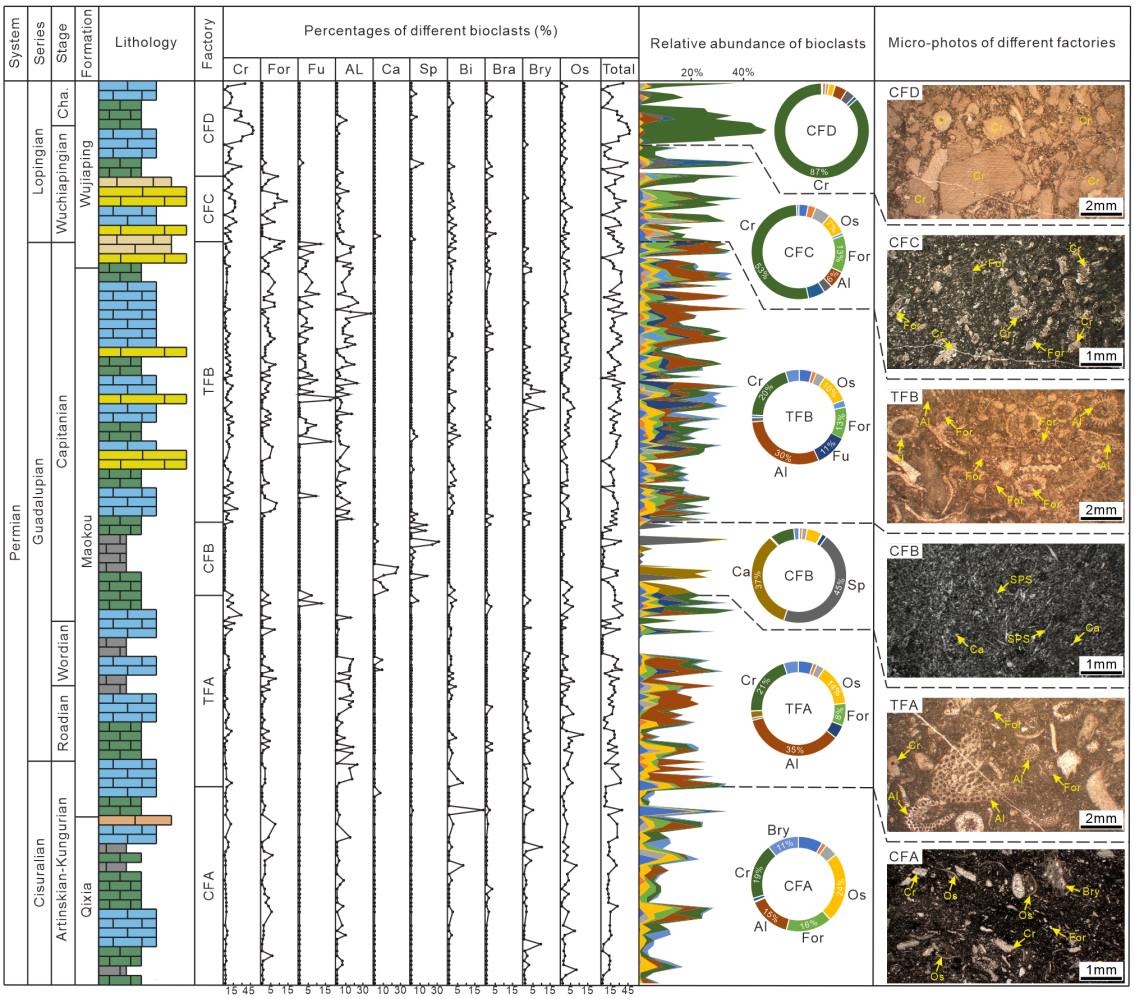

FIGURE 7
The relative abundances of various bioclasts from the Yanduhe section. The pie charts represent the average content of different types of bioclasts in various carbonate factories. CFA, Cool-water factory type A; TFA, Tropical factory type A; CFB, Cool-water factory type B; TFB, Tropical factory type B; CFC, Cool-water factory type C; CFD, Cool-water factory type D; Cha., Changhsingian; Cr, Crinoid; For, Foraminifer; Fu, Fusulinid; AL, Algae; Ca, Calcisphere; Sp, Sponge; Bi, Bivalve; Bra, Brachiopod; Bry, Bryozoan; Os, Ostracods.

4.3.6 Cool-water factory type D

This factory is found in the upper part of the Wujiaping Formation (Late Wuchiapingian to Early Changhsingian age), ranging from the conodont *Clarkina longicuspidata* zone to the *Clarkina subcarinata* zone. This factory type is dominated by crinoids, with minor contributions from ostracods, but lacks fusulinids (Figure 7). Crinoids accounts for 87% of the total of the bioclasts (Figure 7), which are the primary carbonate producers in this factory.

5 Discussion

5.1 Permian sequences and sea-level changes in the Yanduhe section

Eight transgressive-regressive sequences from the Late Artinskian to the Changhsingian can be identified in the Yanduhe section, consistent with previous studies in South China. Specifically, two third-order transgressive-regressive sequences (TR1 and TR2) occurred during the Late Artinskian to Kungurian, three sequences (TR3, TR4, and TR5) during the Kungurian to Capitanian, and three ones (TR6, TR7 and TR8) during the Wuchiapingian to Changhsingian (Figure 3). In the Qixia Formation from the Yanglinqiao section in Zigui County, Hubei Province, two third-order sequences were identified (Wei and Chen, 2011), corresponding to TR1 and TR2 in the Yanduhe section. Similarly, two third-order sequences were recognized in the Qixia Formation from the ST-1 well in northwestern Sichuan Province (Zheng et al., 2018), which align with the findings of this study. Furthermore, three third-order sequences can be identified in the Maokou Formation at the Penglaitan and Tieqiao sections in Laibin City, Guangxi Province (Qiu and Wang, 2010, Qiu et al, 2014), corresponding to TR3, TR4 and TR5 in the Yanduhe section. These sequences were also observed in the Maokou Formation at the Xibeixiang section in Guangyuan City, as well as the Luduba section in Wangcang County, Sichuan Province (Qiu et al., 2024). In addition, three third-order sequences

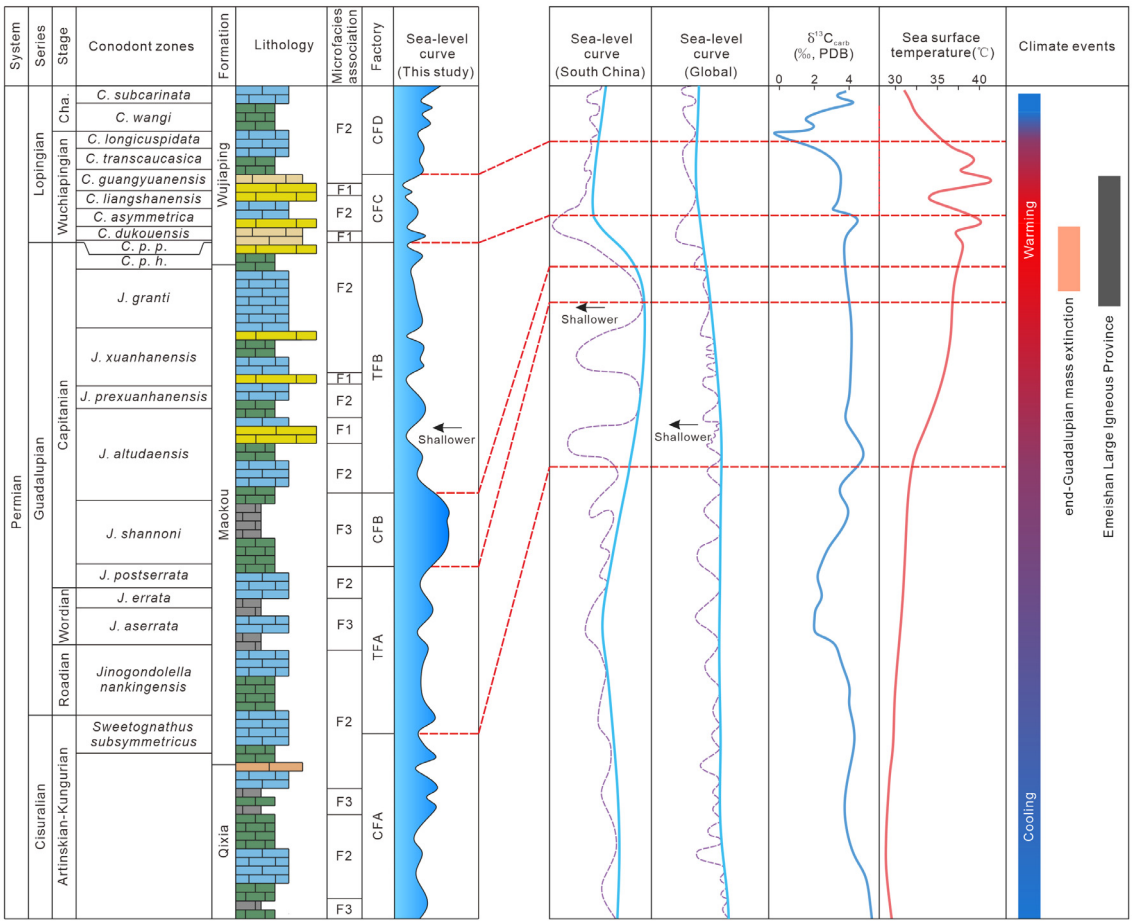

FIGURE 8
The relationship between the carbonate factories from the Yanduhe section with the Permian climate events. Conodont zones are modified after Wu (2020); The timing of the end-Guadalupian mass extinction event is from Shen et al. (2019) and Huang et al. (2019); Emeishan Large Igneous Province interval is from Shellnutt et al. (2020); The Permian sea surface temperature curve is from Chen et al. (2013); The $\delta^{13}C_{carb}$ curve is from Shen et al. (2019); The global sea-level curve is from Haq and Schutter (2008); The sea-level curve of the South China is from Chen et al. (1998); F1~F3 are the same as those in Figure 3; Carbonate factories of CFA, TFA, CFB, TFB, CFC and CFD are the same as those in Figure 7. Cha., Changhsingian; *C.p.p., Clarkina postbitteri postbitteri*; *C.p.h., Clarkina postbitteri hongshuiensis*.

were identified in the Wujiaping Formation from the Yangjiatian section in Jianshi County, Hubei Province (Wei H. Y. et al., 2024), and from the Shuanghui section in Wangcang County, Sichuan Province (Yu, 2023), corresponding to TR6, TR7 and TR8 in this study.

There was a significant regression during the Middle Capitanian; however, sea-level did not change drastically around the Capitanian-Wuchiapingian boundary in the Yanduhe section. The sea-level curve shows a gradual deepening trend beginning in the Roadian of the Guadalupian, reaching a maximum in the Early Capitanian age, followed by a sharp decline in the Middle Capitanian (Figure 7). This trend is consistent with the Permian sea-level changes in South China (Figure 8), which also shows a prominent sea-level regression event in the Middle Capitanian (Wang et al., 1999; Chen et al., 2009; Cheng et al., 2022). Global sea-level begins to decline from the Guadalupian and experiences a sharp decrease from the Capitanian stage to the Wuchiapingian stage (Figure 8) (Haq and Schutter, 2008). However, small fluctuations in sea-level occurred at the Capitanian-Wuchiapingian stage boundary in the Yanduhe section. These fluctuations did not alter the existing sedimentary environment, allowing for continuous carbonate sedimentation. This contrasts with the stratigraphic absence or lithofacies changes observed in the shallow platform (Lai et al., 2008; Zhang et al., 2008; Sun et al., 2010).

5.2 Evolution of the carbonate factory and its driving factors in the Yanduhe section

The concept of the cool-water factory (C-factory) was initially proposed by Schlager (2000), Schlager, 2003). This factory was found in the surface water of middle to high-latitude regions, within upwelling zones, and in deep water below the thermocline in low-latitude regions (Schlager, 2003; Reijmer, 2021; Li et al., 2024). The C-factory's carbonate producers are heterozoans, which include bryozoans, mollusks, and non-fusulinid foraminifers. Notably, this factory does not include tropical grains such as corals and ooids (Schlager, 2003; Reijmer, 2021). Occasionally, algae may also play a significant role as carbonate producers (Schlager, 2003; Reijmer, 2021; Li et al., 2024). In this study, cool-water factory type A and cool-water factory type C are akin to the classical C-factory, with non-fusulinid foraminifers, ostracods, crinoids and bryozoans as the primary carbonate producers. A comparison can also be made with a Permian cool-water factory, which was identified in the Maokou Formation from the Moyang and Nashui sections of Guizhou Province. This Permian factory is characterized by crinoids, bryozoans, and non-fusulinid foraminifers (Meng et al., 2018). Additionally, a cool-water factory in a high-latitude region during the Late Quaternary was dominated by non-fusulinid foraminifers, ostracods, and bryozoans in the Ross Sea region of Antarctica (Melis and Salvi, 2020). Cool-water factory type B in this study is composed of sponges and calcispheres, which is similar to the cool-water factory from the Eucla shelf area of Australia during the early Pleistocene (Saxena and Betzler, 2003). Meanwhile, a Middle Permian cool-water factory contributed by sponges, calcispheres, and non-fusulinid foraminifers has been observed in Moyang and Nashui sections of Guizhou Province (Meng et al., 2018). Cool-water factory type D, discussed in this study, is characterized by a dominance of crinoids, distinguishing it from cool-water factory types A, B and C. Notably, a Late Permian cool-water factory dominated by bryozoans and crinoids had been observed in southern Tibet (Li M. T. et al., 2019). Furthermore, a cool-water factory in the southern Carnarvon Basin of Western Australia was noted for its abundance of gravelly crinoids alongside a smaller presence of bryozoans (Frank et al., 2012).

The tropical factory (T-factory), also originally proposed by Schlager (2000), Schlager, 2003), was found in the surface water of tropical zones (Schlager, 2003; Reijmer, 2021; Li et al., 2024). The carbonate producers associated with the T-factory consist of photozoans, heterozoans, and non-skeletal grains, such as ooids and peloids (Schlager, 2003; Reijmer, 2021; Li et al., 2024). The bioclastic assemblage of fusulinids and algae is typical in Paleozoic tropical warm-water carbonate deposits (Beauchamp, 1994). The tropical factory type A discussed in this study is mainly composed of calcareous algae and ostracods, while the tropical factory type B is predominantly composed of calcareous algae, fusulinids, non-fusulinid foraminifers, and bryozoans. A similar Permian tropical factory characterized by green algae and fusulinids was identified in the Maokou Formation at the Nashui Section of Guizhou Province (Meng et al., 2018). Additionally, a Late Triassic tropical factory dominated by algae, benthic foraminifers, mollusks, and sponges was discovered in the Guanyinya Section of Hanwan Town, Sichuan Province (Liu et al., 2024).

Five significant changes in carbonate factories are observed in the Yanduhe section (Figures 8, 9). The first carbonate factory transition occurred in the Late Kungurian, shifting from the cool-water factory type A to the tropical factory type A (Figures 8, 9). There was no remarkable change in sea-level from the Late Kungurian to Early Capitanian (Figure 3). However, oxygen isotopes began to decrease in South China, indicating an significantly increase in sea surface temperature since the Late Kungurian (Figures 8, 9) (Chen et al., 2013). This increase caused the global climate to transition from an icehouse state to a greenhouse state, ultimately leading to glacial retreat (Montanez et al., 2007; Griffis et al., 2019). A similar change in the carbonate factory was also observed in the Maokou Formation of the Nashui section and the Moyang section in Zunyi, Guizhou Province (Meng et al., 2018). Thus, this carbonate factory transition was mainly controlled by global warming during the the Late Kungurian and Early Roadian.

The second carbonate factory transition took place in the Early Capitanian, shifting from the tropical factory type A to the cool-water factory type B (Figures 8, 9). This change corresponded with an obvious rise in sea-level, in contrast to relatively steady sea surface temperature (Figures 8, 9). Rising sea-levels harmed the shallow-water carbonate factory, resulting in a transformation from a shallow warm-water factory to a deep cool-water factory in this region (Meng et al., 2018).

The third transition appeared during the Middle Capitanian, wherein the cool-water factory type B transitioned to the tropical factory type B (Figures 8, 9). This change was linked to significant

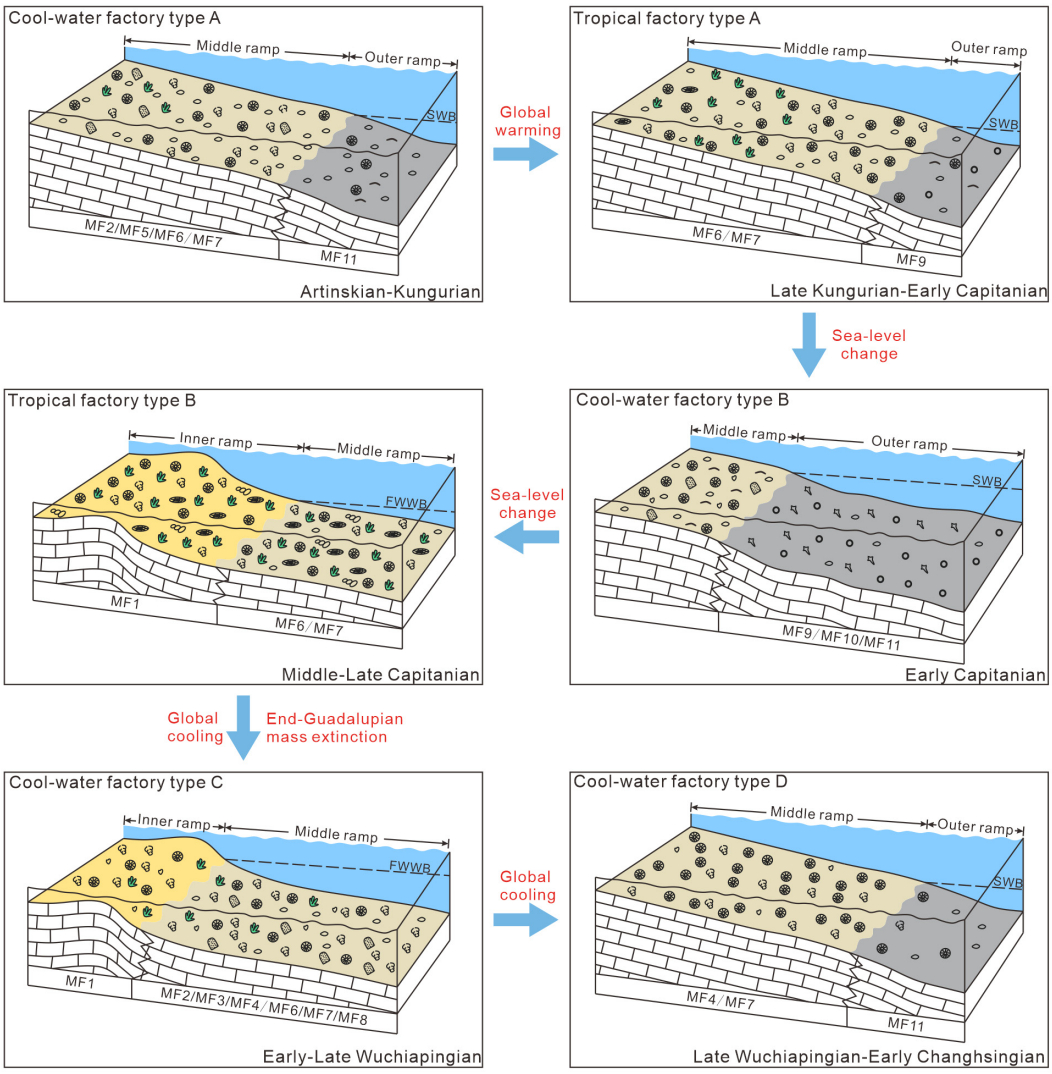

FIGURE 9
Models and controlling factors for the development of various carbonate factories in the Yanduhe section. MF1~MF10 are the same as those in Figure 3; SWB, Storm wave base; FWWB, Fair weather wave base.

regression events (Figures 8, 9), which appears to be a global event (Haq and Schutter, 2008). A shift from deep-water bioclast associations to shallow-water bioclast associations during the Capitanian was also identified at the Tieqiao and Penglaitan sections of Laibin, Guangxi Province (Qiu et al., 2014). In addition, the oxygen isotope studies indicate that there wasn't a notable change in surface seawater temperature from the Wordian to lower-middle Capitanian (Chen et al., 2011, Chen et al., 2013; Wang et al., 2020), suggesting that the third change in the carbonate factory may have been primarily influenced by the decline in sea-level.

The fourth transition of the carbonate factory happened around the boundary between the Capitanian and Wuchiapingian, shifting from the tropical factory type B to the cool-water factory type C (Figures 8, 9). This transformation coincided with a reduction in sea surface temperature and the end-Guadalupian mass extinction event (Figures 8, 9). The end-Guadalupian mass extinction profoundly affected phototrophic organisms such as algae, fusulinids and corals (Isozaki and Aljinovic, 2009; Groves and Wang, 2013). The contents of algae and fusulinids from the Yanduhe section decreased significantly after the Guadalupian-Lopingian boundary (Figure 7), which may be the aftermath of the end-Guadalupian mass extinction. However, the photozoans recovered quickly in the early Wuchiapingian stage (e.g., Qiu and Wang, 2010; Qiu et al., 2014), indicating a transient impact of the mass extinction on the carbonate factory changes. The contents of algae and fusulinids did not recover during the Late Permian, suggesting that the end-Guadalupian mass extinction may not be the sole controlling factor for this carbonate factory change. Notably, there was no significant change in sea-level during this period, suggesting a relatively minor impact on the transition of the carbonate factory by sea-level (Figures 8, 9). Additionally, studies based on oxygen isotopes revealed that there was a significant decrease in sea surface temperatures during the Early

Wuchiapingian (Chen et al., 2013). This drop in temperature might promote cool-water organisms, such as crinoids, thereby contributing to the transition of the carbonate factory.

The fifth transition of the carbonate factory occurred during the Late Wuchiapingian, shifting from the cool-water factory type C to the cool-water factory type D (Figures 8, 9). During this period, the sea-level rose but not significantly (Figures 8, 9). However, a rapid decrease in sea surface temperature during the Late Wuchiapingian implies that this transition was associated with global cooling (Figures 8, 9).

In summary, the first transition is primarily attributed to global warming, whereas the fifth transition is likely driven by global cooling. The fourth transition may be associated with both global cooling and mass extinction events. These three transitions in carbonate factories may reflect the direct impact of the Late Paleozoic climate changes on the marine carbonate production process. Climate change governs seawater temperature and nutrient availability, which regulate the types and habitats of carbonate-producing organisms (Reijmer, 2021; Liu et al., 2024). Rising seawater temperatures promote the proliferation of warm-water organisms, including corals, algae, and fusulinids (e.g., the tropical factory type A in this study), while declining temperatures favor the growth of cool-water organisms such as crinoids and sponges (e.g., the cool-water factory type C and D in this study). This, in turn, affects the production and accumulation of carbonate sediments, ultimately driving shifts in carbonate factory types.

6 Conclusions

1. Ten types of sedimentary microfacies were identified from the Yanduhe section, and grouped into three microfacies associations: inner ramp, middle ramp, and outer ramp.
2. Eight transgressive-regressive sequences from Artinskian to Changhsingian can be identified from the Yanduhe section, and the sequence changes are consistent with previous studies in South China.
3. Six types of carbonate factories and five transitions in carbonate factory are identified from the Yanduhe section. The first and fifth transitions in the carbonate factory are driven by sea surface temperature changes. In contrast, the second and third transitions were caused by local sea-level fluctuations, and the forth transition is attributed to the combined effects of global cooling and the end-Guadalupian mass extinction.

Data availability statement

The original contributions presented in the study are included in the article/Supplementary Material. Further inquiries can be directed to the corresponding author.

Author contributions

ZH: Data curation, Formal Analysis, Methodology, Writing – original draft, Writing – review & editing. XY: Supervision, Writing – original draft, Writing – review & editing. YH: Funding acquisition, Supervision, Validation, Writing – original draft, Writing – review & editing. LT: Funding acquisition, Investigation, Supervision, Writing – original draft, Writing – review & editing. KW: Investigation, Writing – original draft, Writing – review & editing. ML: Writing – original draft, Writing – review & editing.

Funding

The author(s) declare that financial support was received for the research, authorship, and/or publication of this article. This study was funded by the National Key Research and Development Program of China (Grant number 2023YFF0804000), National Natural Science Foundation of China (Grant number 92155201, 42202341), and State Key Laboratory of Biogeology and Environmental Geology, China University of Geosciences (Grant numbers GBL22103).

Conflict of interest

The authors declare that the research was conducted in the absence of any commercial or financial relationships that could be construed as a potential conflict of interest.

Generative AI statement

The author(s) declare that no Generative AI was used in the creation of this manuscript.

Publisher's note

All claims expressed in this article are solely those of the authors and do not necessarily represent those of their affiliated organizations, or those of the publisher, the editors and the reviewers. Any product that may be evaluated in this article, or claim that may be made by its manufacturer, is not guaranteed or endorsed by the publisher.

Supplementary material

The Supplementary Material for this article can be found online at: https://www.frontiersin.org/articles/10.3389/fmars.2025.1513219/full#supplementary-material

References

Beauchamp, B. (1994). Permian climatic coolong in the Canadian Arctic. *Geological Soc. America Special Paper* 288, 229–246. doi: 10.1130/SPE288-p229

Burchette, T. P., and Wright, V. P. (1992). Carbonate ramp depositional systems. *Sedimentary Geology* 79, 3–57. doi: 10.1016/0037-0738(92)90003-A

Chen, Z. Q., George, A. D., and Yang, W. R. (2009). Effects of Middle-Late Permian sea-level changes and mass extinction on the formation of the Tieqiao skeletal mound in the Laibin area, South China. *Aust. J. Earth Sci.* 56, 745–763. doi: 10.1080/08120090903002581

Chen, Z. Q., Jin, Y. G., and Shi, G. R. (1998). Permian transgression-regression sequences and sea-level changes of South China. *Proc. R. Soc. Victoria* 110, 345–367.

Chen, B., Joachimski, M. M., Shen, S. Z., Lambert, L. L., Lai, X. L., Wang, X. D., et al. (2013). Permian ice volume and palaeoclimate history: Oxygen isotope proxies revisited. *Gondwana Res.* 24, 77–89. doi: 10.1016/j.gr.2012.07.007

Chen, B., Joachimski, M. M., Sun, Y. D., Shen, S. Z., and Lai, X. L. (2011). Carbon and condont apatite oxygen isotope records of Guadalupian-Lopingian boundary sections: Climatic or sea-leve signal? *Palaeogeography Palaeoclimatology Palaeoecol.* 311, 145–153. doi: 10.1016/j.palaeo.2011.08.016

Cheng, C., Li, S. Y., Xie, X. Y., Shen, Y. F., Ying, P. L., Manger, W. L., et al. (2022). Sedimentary evolution and sea-level fluctuation of a Paleo-Tethyan Permian carbonate-dominated succession from central China. *Sedimentary Geology* 440, 106244. doi: 10.1016/j.sedgeo.2022.106244

Dunham, R. J. (1962). "Classification of carbonate rocks according to depositional texture," in *Classification of carbonate rocks. A symposium*, vol. 1 . Ed. W. E. Ham (Tulsa: American Association of Petroleum Geologists), 108–121. doi: 10.1306/M1357

Embry, A. F., and Klovan, J. E. (1971). A late Devonian reef tract on northeastern Banks Island, N.W.T. *Bull. Can. Petroleum Geology* 19, 730–781. doi: 10.35767/gscpgbull.19.4.730

Eynattern, V. H., and Dunkl, I. (2012). Assessing the sediment factory: The role of single grain analysis. *Earth-Science Rev.* 115, 97–120. doi: 10.1016/j.earscirev.2012.08.001

Flügel, E. (2004). *Microfacies of carbonate rocks: analysis, interpretation and application* (Berlin, Germany: Springer Science, Business Media), , 1–882.

Frank, T. D., Pritchard, J. M., Fielding, C. R., and Mory, A. J. (2012). Cold-water carbonate deposition in a high-latitude, glacially influenced Permian seaway (Southern Carnarvon Basin, Western Australia). *Aust. J. Earth Sci.* 59, 479–494. doi: 10.1080/08120099.2012.672932

Griffis, N. P., Montanez, I. P., Mundil, R., Richey, J., Isbell, J., Fedorchuk, N., et al. (2019). Coupled stratigraphic and U-Pb zircon age constraints on the late Paleozoic icehouse-to-greenhouse turnover in South-central Gondwana. *Geology* 47, 1146–1150. doi: 10.1130/G46740.1

Groves, J. R., and Wang, Y. (2013). Timing and size selectivity of the Guadalupian (Middle Permian) fusulinoidean extinction. *J. Paleontology* 87, 183–196. doi: 10.2307/23354309

Haq, B. U., and Schutter, S. R. (2008). A chronology of Paleozoic sea-level changes. *Science* 322, 64–68. doi: 10.1126/science.1161648

He, T. C., Wignall, P. B., Newton, R. J., Atkinson, J. W., Keeling, J. F. J., Xiong, Y. J., et al. (2022). Extensive marine anoxia in the European epicontinental sea during the end-Triassic mass extinction. *Global Planetary Change* 210, 103771. doi: 10.1016/j.gloplacha.2022.103771

Hou, Z. S., Shen, S. Z., Henderson, C. M., Yuan, D. X., Zhang, Y. C., and Fan, J. X. (2023). Cisuralian (Early Permian) paleogeographic evolution of South China Block and sea-level changes: Implications for the global Artinskian Warming Event. *Palaeogeogr. Palaeoclimatol. Palaeoecol.* 613, 111395. doi: 10.1016/j.palaeo.2023.111395

Huang, Y. G., Chen, Z. Q., Wignall, P. B., Grasby, S. E., Zhao, L., Wang, X., et al. (2019). Biotic responses to volatile volcanism and environmental stresses over the Guadalupian-Lopingian (Permian) transition. *Geology* 47, 175–178. doi: 10.1130/G45283.1

Isozaki, Y., and Aljinovic, D. (2009). End-Guadalupian extinction of the Permian gigantic bivalve Alatoconchidae: End of gigantism in tropical seas by cooling. *Palaeogeography Palaeoclimatology Palaeoecol.* 284, 11–21. doi: 10.1016/j.palaeo.2009.08.022

Krencker, F. N., Bodin, S., Hofmann, R., Suan, G., Mattiolo, E., Kabiri, L., et al. (2014). The middle Toarcian cold snap: Trigger of mass extinction and carbonate factory demise. *Global Planetary Change* 117, 64–78. doi: 10.1016/j.gloplacha.2014.03.008

Lai, X. L., Wang, W., Wignall, P. B., Bond, D. P. G., Jiang, H. S., Ali, J. R., et al. (2008). Palaeoenvironmental change during the End-Guadalupian (Permian) mass extinction in Sichuan, China. *Palaeogeograpyh Palaeoclimatology Palaeoecol.* 269, 78–93. doi: 10.1016/j.palaeo.2008.08.005

Laugie, M., Michel, J., Pohl, A., Poli, E., and Borgomano, J. (2019). Global distribution of modern shallow-water marine carbonate factories: a spatial model based on environmental parameters. *Sci. Rep.* 9, 16432. doi: 10.1038/s41598-019-52821-2

Lehrmann, D. J., Stepchinski, L. M., Wolf, H. E., Li, L. Z., Li, X. W., Minzoni, M., et al. (2022). The role of carbonate factories and sea water chemistry on basin-wide ramp to high-relief carbonate platform evolution: Triassic, Nanpanjiang Basin, South China. *Depositional Rec.* 8, 186–418. doi: 10.1002/dep2.166

Lei, H., Huang, W. H., Jiang, Q. C., and Luo, P. (2024). Siliceous deposition in limestone-marl alternations of the Yangtze Carbonate Platform during the Permian Chert Event. *Palaeogeography Palaeoclimatology Palaeoecol.* 651, 112382. doi: 10.1016/j.palaeo.2024.112382

Lestari, W., Al-Suwaidi, A., Fox, C. P., Vajda, V., and Hennhoefer, D. (2024). Carbon cycle perturbations and environmental change of the Middle Permian and Late Triassic Paleo-Antarctic circle. *Sci. Rep.* 14, 9742 doi: 10.1038/s41598-024-60088-5

Li, F., Gong, Q. L., Burne, R. V., Tang, H., Su, C. P., Zeng, K., et al. (2019). Ooid factories operating under hothouse conditions in the earliest Triassic of South China. *Global Planetary Change* 172, 336–354. doi: 10.1016/j.gloplacha.2018.10.012

Li, M. T., Song, H. J., Woods, A. D., Dai, X., and Wignall, P. B. (2019). Facies and evolution of the carbonate factory during the Permian–Triassic crisis in South Tibet, China. *Sedimentology* 59, 646–678. doi: 10.1111/sed.12619

Li, M. T., Tian, L., Wignall, P. B., Dai, X., Lin, W., Cai, Q. S., et al. (2023). Expansion of microbial-induced carbonate factory into deeper water after the Permian-Triassic mass extinction. *Global Planetary Change* 230, 104274. doi: 10.1016/j.gloplacha.2023.104274

Li, F., Wang, X., and Yan, J. X. (2024). From "Facies Model" to "Carbonate Factory": Conceptual framework and development directions of the carbonate factories. *Acta Sedimentologica Sin.* 42, 343–350. doi: 10.14027/j.issn.1000-0550.2024.050

Liu, J. J., Wang, X., Meng, L. Z., Zhen, Y. H., Feng, Y. Y., Jin, X., et al. (2024). Quantitative study on the composition and evolution of the Late Triassic Carnian shallow-water carbonate factories in Northwestern Sichuan. *Acta Sedimentologica Sin.* 42, 445–465. doi: 10.14027/j.issn.1000-0550.2023.121

Liu, Z. C., Zhou, Q., Liu, K., Wang, Y., Chen, D., Chen, Y. M., et al. (2023). Sedimentary features and paleogeographic evolution of the Middle Permian Trough Basin in Zunyi, Guizhou, South China. *J. Earth Sci.* 34, 1803–1815. doi: 10.1007/s12583-021-1406-2

Marchetti, L., Forte, G., Kustatscher, E., DiMichele, W. A., Lucas, S. G., Roghi, G., et al. (2022). The Artinskian Warming Event: An euramerican change in climate and the terrestrial biota during the Early Permian. *Earth-Science Rev.* 226, 103922. doi: 10.1016/j.earscirev.2022.103922

Melis, R., and Salvi, G. (2020). Foraminifer and ostracod occurrence in a cool-water carbonate factory of the Cape Adare (Ross Sea, Antarctica): A key lecture for the climatic and oceanographic variations in the last 30000 years. *Geosciences* 10, 413–441. doi: 10.3390/geosciences10100413

Meng, Q., Huang, H., Yan, J. X., and Chen, F. Y. (2018). Sedimentary evolution of the Middle Permian carbonate platform margin in southern Guizhou and its palaeo-oceanographic implications. *J. Palaeogeogr.* 20, 87–103. doi: 10.7605/gdlxb.2018.01.006

Meng, Q., Xue, W. Q., Chen, F. Y., Yan, J. X., Cai, J. H., Sun, Y. D., et al. (2022). Stratigraphy of the Guadalupian (Permian) siliceous deposits from central Guizhou of South China: Regional correlations with implications for carbonate productivity during the Middle Permian biocrisis. *Earth-Science Rev.* 228, 104011. doi: 10.1016/j.earscirev.2022.104011

Michel, J., Laugié, M., Pohl, A., Lanteaume, C., Masse, J.-P., Donnadieu, Y., et al. (2019). Marine carbonate factories: a global model of carbonate platform distribution. *Int. J. Earth Sci.* 108, 1773–1792. doi: 10.1007/s00531-019-01742-6

Montanez, I. P., Tabor, N. J., Niemeier, D., Dimichele, W. A., Frank, T. D., Fielding, C. R., et al. (2007). CO_2-Forced climate and vegetation instability during Late Paleozoic Deglaciation. *Science* 315, 87–91. doi: 10.1126/science.1134207

Morabito, C., Papazzoni, C. A., Lehrmann, D. J., Payne, J. L., Ai-Ramadan, K., and Morsilli, M. (2024). Carbonate factory response through the MECO (Middle Eocene Climate Optimum) event: Insight from the Apulia Carbonate Platform, Gargano Promontory, Italy. *Sedimentary Geology* 461, 106575. doi: 10.1016/j.sedgeo.2023.106575

Pomar, L., and Hallock, P. (2008). Carbonate factories: A conundrum in sedimentary geology. *Earth-Science Rev.* 87, 134–169. doi: 10.1016/j.earscirev.2007.12.002

Pomar, L., and Haq, B. U. (2016). Decoding depositional sequences in carbonate systems: Concepts vs experience. *Global Planetary Change* 146, 190–225. doi: 10.1016/j.gloplacha.2016.10.001

Qiu, Z., Dou, L. R., Wu, J. F., Wei, H. Y., Liu, W., Kong, W. L., et al. (2024). Lithofacies palaeogeographic evolution of the Middle Permian sequence stratigraphy and its implications for Shale Gas exploration in the Northern Sichuan and Western Hubei Provinces. *Earth Sci.* 49, 712–748. doi: 10.3799/dqkx.2023.216

Qiu, Z., and Wang, Q. C. (2010). Middle and Upper Permian sedimentary microfacies in the Tieqiao Section in Laibin, Guangxi, China. *Acta Sedimentologica Sin.* 28, 1020–1036. doi: 10.14027/j.cnki.cjxb.2010.05.008

Qiu, Z., Wang, Q. C., Zou, C. N., Yan, D. T., and Wei, H. Y. (2014). Transgressive–regressive sequences on the slope of an isolated carbonate platform (Middle–Late Permian, Laibin, South China). *Facies* 60, 327–245. doi: 10.1007/s10347-012-0359-4

Reijmer, J. J. G. (2021). Marine carbonate factories: Review and update. *Sedimentology* 68, 1729–1796. doi: 10.1111/sed.12878

Saxena, S., and Betzler, C. (2003). Genetic sequence stratigraphy of cool water slope carbonates (Pleistocene Eucla Shelf, southern Australia). *Int. J. Earth Sci.* 92, 482–493. doi: 10.1007/s00531-003-0338-7

Schlager, W. (2000). *Sedimentation rates and growth potential of tropical, cool-water and mud-mound carbonate systems* (London: Geological Society, Special Publications), 217–227.

Schlager, W. (2003). Benthic carbonate factories of the Phanerozoic. *Int. J. Earth Sci.* 92, 445–464. doi: 10.1007/s00531-003-0327-x

Shellnutt, J. G., Pham, T. T., Denyszyn, S. W., Yeh, M. W., and Tran, T. A. (2020). Magmatic duration of the Emeishan large igneous province: Insight from northern Vietnam. *Geology* 48, 457–461. doi: 10.1130/G47076.1

Shen, S. Z., Yuan, D. X., Henderson, C. M., Wu, Q., Zhang, Y. C., Zhang, H., et al. (2020). Progress, problems and prospects: An overview of the Guadalupian Series of South China and North America. *Earth-Science Rev.* 211, 103412. doi: 10.1016/j.earscirev.2020.103412

Shen, S. Z., and Zhang, H. (2017). What caused the five mass extinctions? *Chin. Sci. Bull.* 62, 1119–1135. doi: 10.1360/N972017-00013

Shen, S. Z., Zhang, F. F., Wang, W. Q., Wang, X. D., Fan, J. X., Chen, J. T., et al. (2024). Deep-time major biological and climatic events versus global changes: Progresses and challenges. *Chin. Sci. Bull.* 69, 268–285. doi: 10.1360/TB-2023-0218

Shen, S. Z., Zhang, H., Zhang, Y. C., Yuan, D. X., Chen, B., He, W. H., et al. (2019). Permian integrative stratigraphy and timescale of China. *Sci. China Earth Sci.* 62, 154–188. doi: 10.1007/s11430-017-9228-4

Song, H. Y., Algeo, T. J., Song, H. J., Tong, J. N., Wignall, P. B., Bond, D. P. G., et al. (2023). Global oceanic anoxia linked with the Capitanian (Middle Permian) marine mass extinction. *Earth Planetary Sci. Lett.* 610, 118128. doi: 10.1016/j.epsl.2023.118128

Sun, Y. D., Lai, X. L., Wignall, P. B., Widdowson, M., Ali, J. R., Jiang, H. S., et al. (2010). Dating the onset and nature of the Middle Permian Emeishan large igneous province eruptions in SW China using conodont biostratigraphy and its bearing on mantle plume uplift models. *Lithos* 119, 20–33. doi: 10.1016/j.lithos.2010.05.012

Wang, W. Q., Garbelli, C., Zhang, F. F., Zheng, Q. F., Zhang, Y. C., Yuan, D. X., et al. (2020). A high-resolution Middle to Late Permian paleotemperature curve reconstructed using oxygen isotopes of well-preserved brachiopod shells. *Earth Planetary Sci. Lett.* 540, 116245. doi: 10.1016/j.epsl.2020.116245

Wang, X. D., and Jin, Y. G. (2000). Permian palaeogeographic evolution of the Jiangnan Basin, South China. *Palaeogeogr. Palaeoclimatol. Palaeoecol.* 160, 35–44. doi: 10.1016/S0031-0182(00)00043-2

Wang, C. S., Li, X. H., Chen, H. D., and Qin, J. X. (1999). Permian sea-level changes and rising-falling events in South China. *Acta Sedimentologica Sin.* 17, 39–44. doi: 10.14027/j.cnki.cjxb.1999.04.005

Wang, X., Meng, L. Z., Liu, J. J., Ning, M., Ge, Y. Z., Zeng, Y. H., et al. (2024). Detailed characterization of carbonate factories from the perspective of quantitative reconstruction. *Acta Sedimentologica Sin.* 42, 351–370. doi: 10.14027/j.issn.1000-0550.2024.047

Wang, J. Y., Tarham, L. G., Jacobson, A. D., Oehlert, A. M., and Planavsky, N. J. (2023). The evolution of the marine carbonate factory. *Nature* 615, 265–269. doi: 10.1038/s41586-022-05654-5

Wang, W. Q., Zhang, F. F., Zhang, S., Cui, Y., Zheng, Q. F., Zhang, Y. C., et al. (2023). Ecosystem responses of two Permian biocrises modulated by CO_2 emission rates. *Earth Planetary Sci. Lett.* 602, 117940. doi: 10.1016/j.epsl.2022.117940

Wei, C., Cao, J., Dong, T., and Wang, Y. (2024). Effects of the Emeishan large igneous province (ELIP) and coastal upwelling on paleoenvironment and organic matter accumulation during the Middle Permian (Capitanian), South China. *Palaeogeography Palaeoclimatology Palaeoecol.* 653, 112426. doi: 10.1016/j.palaeo.2024.112426

Wei, H. Y., and Chen, D. Z. (2011). Lithofacies palaeogeography of the Qixia Age of Permian in western Hubei-northwestern Hunan Provinces. *J. Palaeogeogr.* 13, 551–562.

Wei, H. Y., Hu, D., Qiu, Z., Zhang, X., Liu, W., Kong, W. L., et al. (2024). Sedimentological and geochemical characteristics of Late Permian Organic-Rich rocks in North Sichuan and West Hubei Province. *Acta Sedimentologica Sin.* 42, 774–798.

Wei, H. Y., Wei, X. M., Qiu, Z., Song, H. Y., and Shi, G. (2016). Redox conditions across the G-L boundary in South China: Evidence from pyrite morphology and sulfur isotopic compositions. *Chem. Geology* 440, 1–14. doi: 10.1016/j.chemgeo.2016.07.009

Wu, K. (2020). "Conodont biostratigraphy and morphologic variation from the middle permian to lower triassic of south China," in *China university of geosciences. Dissertation wuhan* (Wuhan, China: China University of Geosciences).

Yu, Y. M. (2023). "Controlling factors of source rock development and distribution in the middle upper permian, northeastern sichuan basin," in *China university of petroleum. Dissertation beijing* (Beijing, China: China University of Petroleum).

Zhang, L. L., Zhang, N., and Xia, W. C. (2008). Conodont succession in the Guadalupian-Lopingian boundary interval (Upper Permian) of the Maoershan section, Hubei Province, China. *Micropaleontology* 53, 433–446. doi: 10.2113/gsmicropal.53.6.433

Zheng, C., Wang, Y. F., Tang, X. Y., Hu, X., and Sun, Z. Y. (2018). Sequence stratigraphic division and sedimentary facies analysis of Qixia Formation in the Shuangyushi Block. *Special Oil Gas Reservoirs* 25, 39–45. doi: 10.3969/j.issn.1006-6535.2018.04.008